Proceedings of Global Power and Propulsion Society
ISSN-Nr: 2504-4400
GPPS Hong Kong 2023
October 17-19, 2023
www.gpps.global

GPPS-TC-2023-0117

Adjusting the Ratio of Steady and Dynamic Components of Total Pressure Distortion Using the Combination of Annular Plate and Cylindrical Rod

Enbo Sun
Xi'an Jiaotong University
sunenbo@stu.xjtu.edu.cn
Xi'an, Shaanxi, P.R.China

Haideng Zhang
Airforce Engineering University
zhanghaideng@126.com
Xi'an, Shaanxi, P.R.China

Yun Wu
Airforce Engineer University
Xi'an Jiaotong University
wuyun1223@126.com
Xi'an, Shaanxi, P.R.China

Shanzhen Li
Xi'an Jiaotong University
1021678293@qq.com
Xi'an, Shaanxi, P.R.China

Yuhan Long
Xi'an Jiaotong University
1637170145@qq.com
Xi'an, Shaanxi, P.R.China

ABSTRACT

The aero-engine always suffers from the inlet distortion because of intake flow separation and wing wake during the aircraft flight. Total pressure distortion, which has negative impact on the stability of the compressor, is a typical form of inlet distortion. The test and analysis of the compressor stability under the inlet total pressure distortion is an important segment in aero-engine design. The inlet total pressure distortion consists of steady and dynamic components, and the ratio of steady and dynamic components will change with the variance of working conditions. However, the traditional distortion generator can only generate the inlet total pressure distortion with fixed steady/dynamic ratio (SDR), and this makes it difficult to test the performance of aero-engines under different types of inlet total pressure distortions. To solve this problem, a new-type total pressure distortion generator based on the combination of cylindrical rod/annular plate and baffle plate is designed in this paper. Through adjusting the characteristic parameters of the rod/plate, the SDR of total pressure distortion can be varied actively. The wind tunnel test results show that increasing the number of the cylindrical rods, the circumferential scale of the annular plate and the height of the rods/plates can reduce the SDR.

INTRODUCTION

Inlet total pressure distortion is a common issue in modern aircraft engine design. Flow distortion always comes from the flow separation, such as boundary layer ingestion, lip separation, shock induced separation and secondary internal flows (Tanguy et al., 2018). The inlet total pressure distortions can be summarized as steady-state distortion (Longley and Greitzer, 1992; Anderson and Gibb, 1998; Mistry and Pradeep, 2013) and dynamic distortion (Gil-Prieto et al., 2018; Gil-Prieto et al., 2019; Xu et al., 2021) according to whether the distorted inlet flow changes with time or not.

Mesh screen is one of the earliest steady-state total pressure distortion generator. The screen comprises of different meshes and shapes to reach the target total pressure patterns. The target pressure losses are dependent on the selection of the density and number of overlapping screens(Smith Jr, 1996; SAE, 2017). Another distortion generator in Ref (Van Deusen and Mardoc, 1972) is also used to generate steady-state distortion pattern. It has movable parts to provide the ability of generating different patterns during one test. AEDC also developed Air Jet Distortion Generator (AJDG) to generate steady-state distortion patterns (Overall, 1976; Overall and Harper, 1977; Hubble and Smith, 1979). This generator uses an array of secondary air jets mounted upstream of the engine. Each jet can induce a local total pressure drop through a momentum exchange between the jet and the main flow.

In 1960s, Researchers of NASA Lewis Research Center proved that fluctuating pressure caused engine stall first time during an AEDC test of a J93 engine with the B70 inlet (Bowditch and Coltrin, 1983). As time-variant distortion began to introduce an entirely new set of stability problems, different distortion simulators for generating dynamic total-pressure

distortion have been developed. Applying shock wave and boundary layer interaction (SWBLI) is a way to generate dynamic distortion at random frequencies. AEDC has designed a generator using SWBLI to generate dynamic distortion (Kimzey, 1965; Oates et al., 1969; Plourde and Brimelow, 1969). This scheme consists of a movable centerbody inside a venturi, and the wave structure develops inside the venturi by moving the plug axially. General Electric Company (GE) proposes another scheme to simulate both spatial and temporal total pressure distortion characteristics (Brimelow et al., 1974; Anderson, 1983). The device consists of a square channel and wall composed of variable ramps. The random-frequency total pressure fluctuations are induced by SWBLI when the ramp is at different positions, and the spatial distortion comes from the asymmetrical positioning of the ramps. Some Discrete Frequency Distortion Generators using rotatable parts and stational parts are also designed (Lazalier and Tate, 1970; Kutschenreuter JR et al., 1974). The frequency of time-variant distortion is decided by the speed of the rotor, and the amplitude is related to the characteristics of stators and rotors. Virginia Tech and AEDC have proposed a dynamic total-pressure distortion generator (DiPietro, 1996; Eddy, 2001; Cramer, 2002). This generator uses an array of porous blockage elements that control the target distortion pattern by opening and closing the blockage elements. The magnitude of the total pressure distortion is related to the porous blockage element's opening angle. The Central Institute of Aviation Motors (CIAM) in Russa used a pair of baffle plates positioned in the engine inlet flow to generate dynamic total pressure distortion by hydraulically powered (Smith JR, 1996).

In fact, the steady and dynamic components of total pressure distortion are presence at the inlet of aircraft engine simultaneously. The baffle's distortion characteristic is similar to the realistic flight conditions. However, the ratio of steady-state to dynamic distortion is always changing corresponding to the level of separation. The single baffle distortion generator can only generate a distortion pattern with a fixed ratio.

METHODOLOGY

Test bed

The test was carried out on the indraft wind tunnel test rig in Figure 1, which consists of a 110kW centrifugal compressor, inlet system, distortion generator installations, turbulent development section and measurement system.

During the test, the air flows through the dust cover, bell mouth and inlet section. The dust cover is designed to protect the aerodynamic probe from the damage of dust. The inlet Mach number is monitored using a pitot probe. Diameter of the wind tunnel is 380mm, and the total length of the wind tunnel is 1650mm.

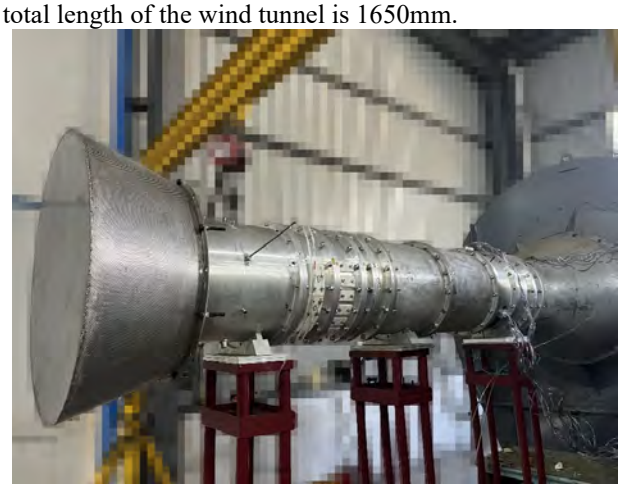

Figure 1 The indraft wind tunnel test rig

The baffle distortion generator is located 950mm upstream of the aerodynamic interface plane (AIP). The adjustable parts, which are designed to install the cylindrical rods and annular plates, are located 277.5mm and 135mm upstream of the baffle distortion generator, respectively. Then the baffle plate and the cylindrical rods or annular plate constitute the combinational distortion generator. Geometrical parameters of the cylindrical rods and annular plates can be changed to generate different types of inlet total pressure distortions. The relative depth of the baffle is 30%. The combinational distortion generator is shown in Figure 2.

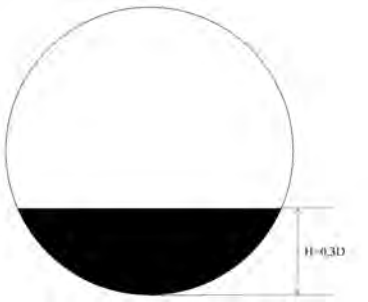

(a) Baffle distortion generator

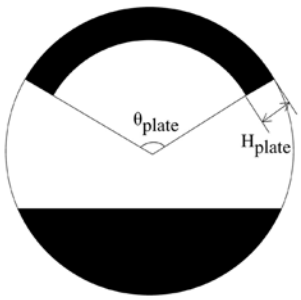

(b) Annular plate-baffle distortion generator (APBDG)

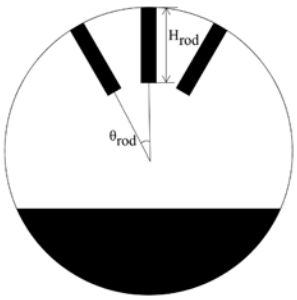

(c) Cylindrical rod-baffle distortion generator (CRBDG)

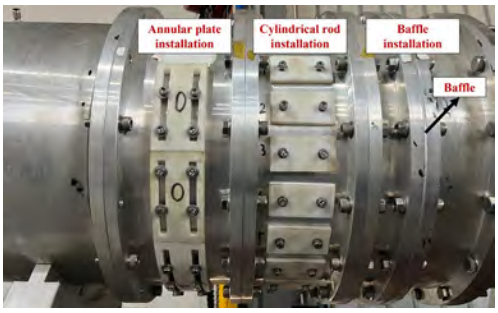

Distortion generator installation

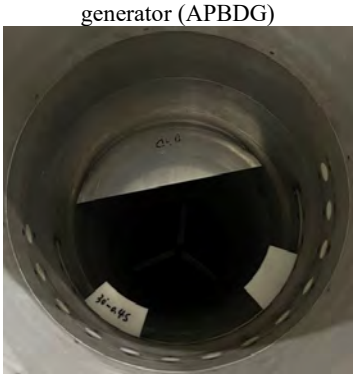

Annular plate-baffle distortion generator (APBDG)

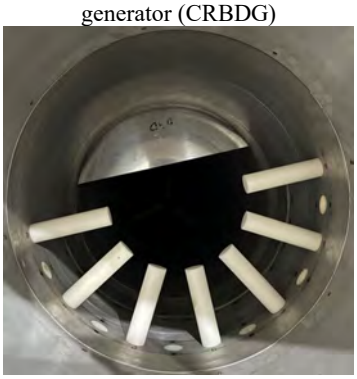

Cylindrical rod-baffle distortion generator (CRBDG)

Figure 2 Total pressure distortion generator diagram

Table 1 shows the geometrical parameters of the combination distortion generators.

Design parameters	Unit	Values
Relative insertion depth of baffle	mm	0.3D
Distance between annular plate and baffle	mm	135
Distance between cylindrical rod and baffle	mm	277.5
Height of annular plate	mm	20, 43
Circumferential angle of annular plate	degree	60, 120, 180
Height of cylindrical rod	mm	20, 60, 100
Number of cylindrical rod	-	3, 5, 7

Test scheme

Figure 3 shows measurement scheme of the research. Three dynamic total pressure rakes are used to measure the total pressure distortion. Their circumferential spacing maintains at 120 degrees. Along the circumferential direction, the rakes move Δθ (=15°) each step. For each dynamic sensor, the radial distance between each other is Δr (=11mm). The total radial number and circumferential step numbers are 8 and 8 respectively. This results in 8 radial measurement points and 8 circumferential measurement points for each rake. There are in total 8×8×3=192 measurement points. The dynamic pressure sensor has a sampling frequency of 10kHz, and the sampling time is not less than 10s.

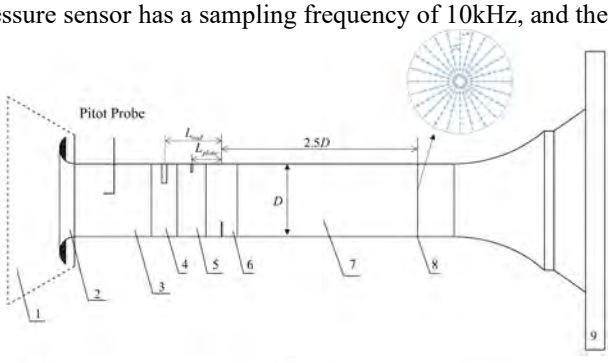

1.Dust cover
2.Bell mouth
3.Inlet section
4.Cylindrical rods installation section
5.Annular plate installation section
6.Baffle installation section
7.Turbulence development section
8.AIP section
9.Centrifugal compressor

(a) Location diagram of each installation section

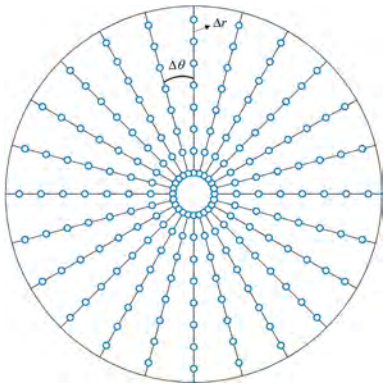

(b) Measurement point layout

Figure 3 Diagram of the measurement scheme

Methods to evaluate total pressure distortion

The evaluation metrics utilized to assess distortion intensity at the AIP section comprise the total pressure recovery coefficient σ, the steady-state circumferential total pressure distortion descriptor $\Delta\sigma$, the surface mean turbulence ε_{av}, and the complex distortion descriptor W.

The total pressure recovery coefficient σ is defined as:

$$\sigma = \frac{P_2^*}{P_1^*} \qquad (1)$$

Where P_1^* is the total pressure of inlet flow, and P_2^* is the local total pressure.

In this study, to investigate the relationship between the distortion descriptors and the geometrical parameters, the inlet dynamic pressure $0.5\rho V_{in}^2$ is employed as the denominator instead of the surface average total pressure P_{2av}^* at the AIP, where ρ is the density of air, V_{in} is the axial velocity. Altering the denominator is due to the low Mach number of wind tunnel inflow (0.15-0.22), which results in the distortion descriptor magnitude of only 0.01.

The steady-state circumferential total pressure distortion descriptor $\Delta\sigma$ is defined as:

$$\Delta\sigma = \frac{P_{2av}^* - P_{0av}^*}{0.5\rho V_{in}^2} \qquad (2)$$

Where P_{0av}^* is the average total pressure of low-pressure region.

The surface average turbulence ε_{av} is defined as:

$$\varepsilon_{av} = \frac{1}{\mathrm{N}}\sum_{i=1}^{N}\varepsilon(i) \qquad (3)$$

Where N is the number of points for measuring turbulent total pressure, $\varepsilon(i)$ is the turbulence of the *i*th turbulent total pressure measurement point.

$\varepsilon(i)$ is defined as:

$$\varepsilon(i) = \frac{\left(\Delta P_2^*\right)_{RMS}}{0.5\rho V_{in}^2} \qquad (4)$$

Where $\left(\Delta P_2^*\right)_{RMS}$ is the root mean square of the turbulent total pressure

$$\left(\Delta P_2^*\right)_{RMS} = \sqrt{\frac{1}{T_u}\int_0^{T_u}\left(P_2^*(t) - P_{2av}^*\right)^2 dt} \qquad (5)$$

Where $P_2^*(t)$ is the time-variant total pressure measured by dynamic pressure sensors, and T_u is the sampling time of high-frequency pressure sensors.

The complex total pressure distortion descriptor W represents the non-uniformity of the flow field at the AIP, expressed as a linear combination of the steady-state distortion descriptor and the dynamic distortion descriptor.

$$\mathrm{W} = \Delta\sigma + \varepsilon_{av} \qquad (6)$$

RESULTS AND DISCUSSION

Experimental validation

Using dynamic pressure sensors embedded within the measuring rakes radially has posed a challenge in calibrating the test results. Recent studies have indicated that implementing five-hole probes can precisely measure the distorted flow field's steady-state total pressure and swirl angle characteristics. Figure 4(a) portrays the baffle distortion generator's total pressure recovery coefficient pattern, and the baffle's relative height is 0.2D. It is the pattern measured by dynamic pressure measuring rakes.

Figure 4(b) illustrates the five-hole probes' total pressure recovery coefficient pattern. Notably, the high-pressure and transition regions of the two maps are fundamentally consistent. Although the five-hole probes' low-pressure region range is marginally greater than that measured by the dynamic pressure measuring rakes, the five-hole probes exhibit a higher resolution because of more radial measuring points in the low-pressure region. The average surface total pressure recovery coefficient determined by the dynamic measurement rakes is 0.9946, whereas the evaluation coefficient calculated by the five-hole probes is 0.9938, resulting in a negligible 0.08% deviation.

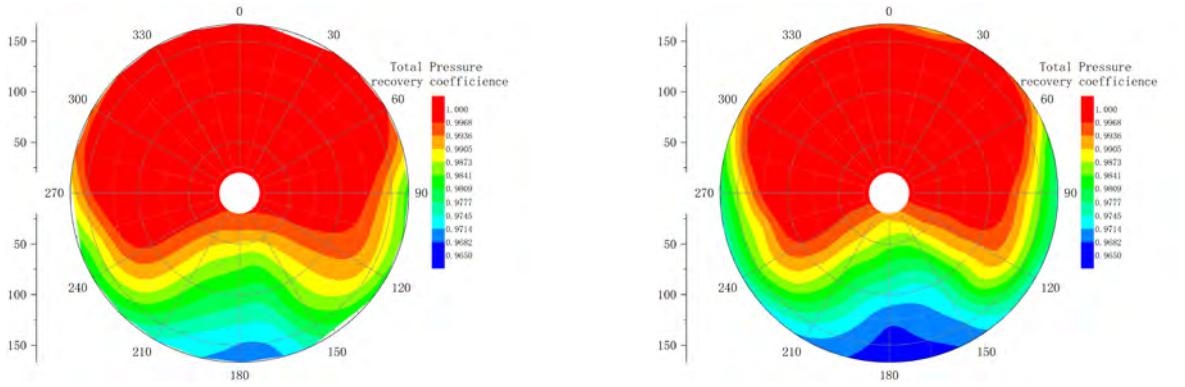

(a) The map measured by dynamic pressure rakes (b) The map mesured by five-hole probes

Figure 4 Total pressure recovery coefficient patterns

Distortion flow characteristics of baffle distortion generator

The present study involves a baffle distortion generator with a relative height of 0.3D, and a centrifugal fan frequency of 42Hz for experimental measurements. The total pressure recovery coefficient map at the AIP depicts a distorted flow field comprising three discernible regions, i.e., the high-pressure region above, the low-pressure region below, and the transition region between the high-pressure region and low-pressure region. The high-pressure zone exhibits robust flow capacity and negligible pressure pulsation. The obstruction caused by the baffle distortion generator leads to low-energy fluid in the low-pressure zone, making it challenging to exchange momentum with the fluid in the primary flow zone, resulting in relatively low turbulence intensity. The transition zone, formed by continuous shear between the mainstream fluid and the baffle plate's edge, is characterized by a large number of shedding vortices at the edge of the baffle plate, leading to considerable pressure fluctuations and a high turbulence region in the transition zone.

The steady-state distortion descriptor of the flow field is larger than the turbulence intensity, and the ratio of the steady and dynamic components of total pressure distortion is approximately 1.6.

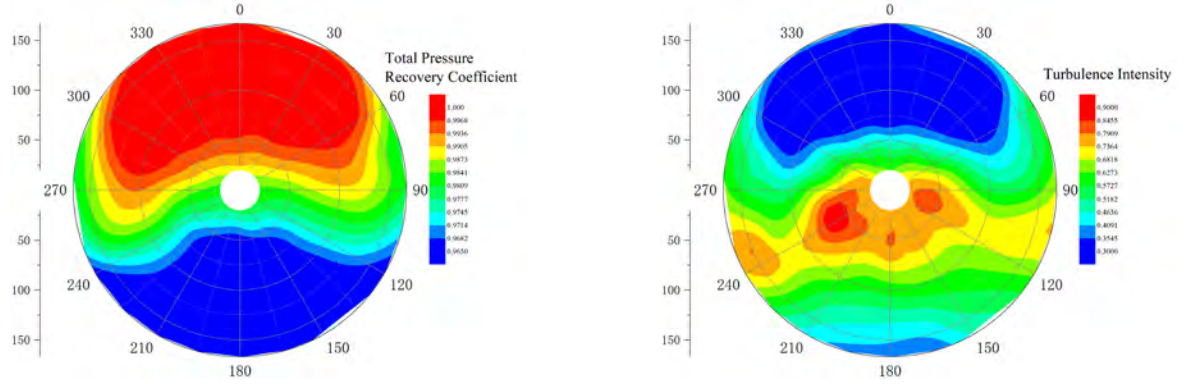

(a) Total pressure recovery coefficient pattern (b) Turbulence pattern

Figure 5 Total pressure distortion pattern generated by baffle distortion generator

EFFECT OF ANNULAR PLATE ON DISTORTION DESCRIPTOR

The patterns depicting the total pressure recovery coefficient of Figure 5 suggest that the high-pressure region above the baffle plate exhibits robust flow capacity, thereby causing minimal pressure fluctuations and correspondingly low turbulence intensity. In order to modify the steady/dynamic distortion ratio at the AIP section, the design philosophy of the combined distortion generator involves incorporating annular plates or cylindrical rods to alter the total pressure distribution and pressure pulsations within the high-pressure region.

Effect of the annular plate's height on the distortion descritor

Figure 6 illustrates the changes in the steady-state distortion descriptor and turbulence of the APBDG comprising annular plates with circumferential angles of 60°, 120°, and 180°. As shown in the figure, the steady distortion descriptor and turbulence all increase with the annular plate's height. The dynamic distortion component's increasing rate is higher than the steady distortion component, which means that adding annular plate in front of the baffle can decrease the ratio of the steady and dynamic distortion components.

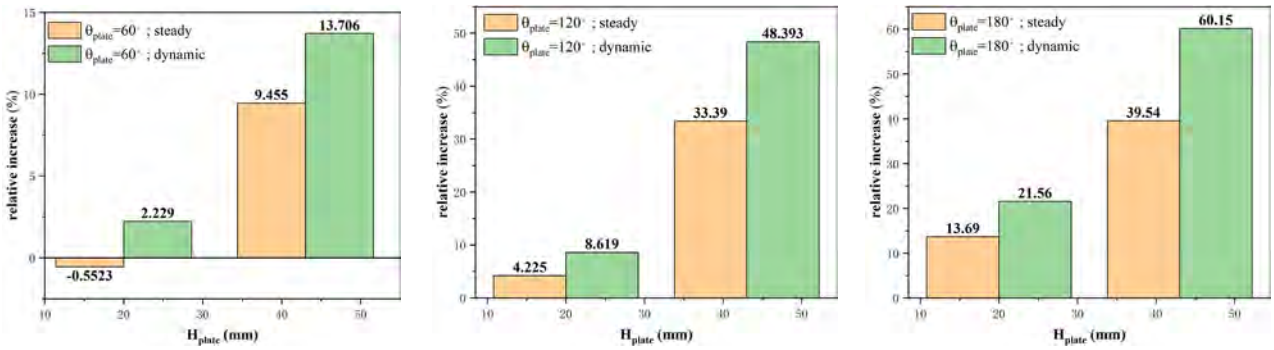

Figure.6 The influence of annular plate height on the distortion descriptor's relative increase

As shown in Figure.7, adding annular plates can improve the distortion generator's ability to generate stronger turbulence. The ratio of steady and dynamic components of total pressure distortion is reduced by 12.9% maximally at the height of 43mm.

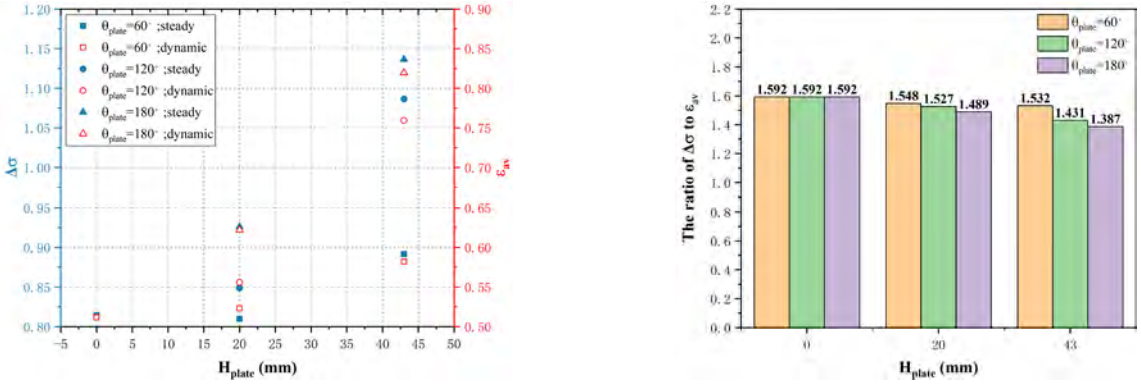

Figure.7 Effect of annular plate heights on the distortion descriptor

Figure.8 displays the APBDG's total pressure recovery coefficient and turbulence patterns at different annular plate heights. Compared to Figure.5, results show that increasing the annular plate height expands the low-pressure area behind the baffle and splits the high-pressure region into smaller regions. The middle section of the high-pressure region forms a relatively lower and smaller total pressure area, and the flow field's pulsation in the high-pressure region intensifies.

The throat consisting of the annular plate and the baffle accelerates the fluid flow, inducing stronger pressure pulsations and increasing turbulence intensity in the transition region. As the annular plate height increases, the range of high turbulence areas in the high-pressure and transition regions also grows.

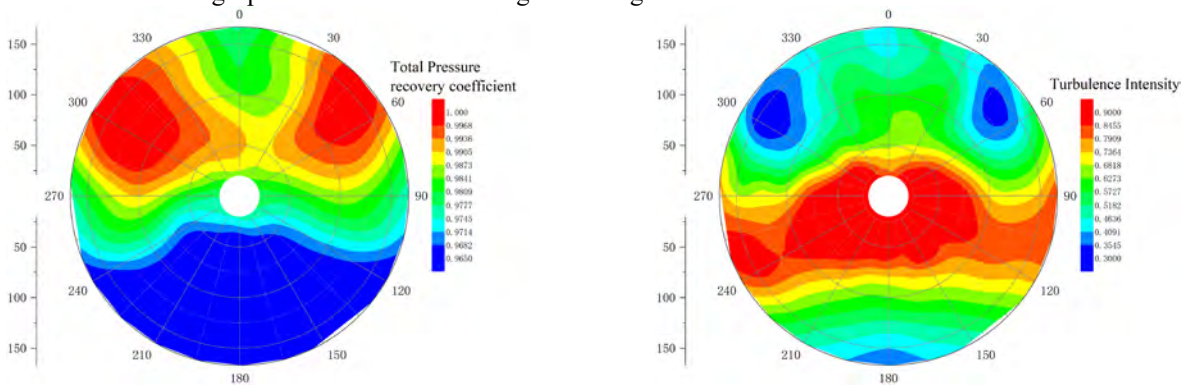

(a) H_{plate}=20mm, θ_{plate}=120°

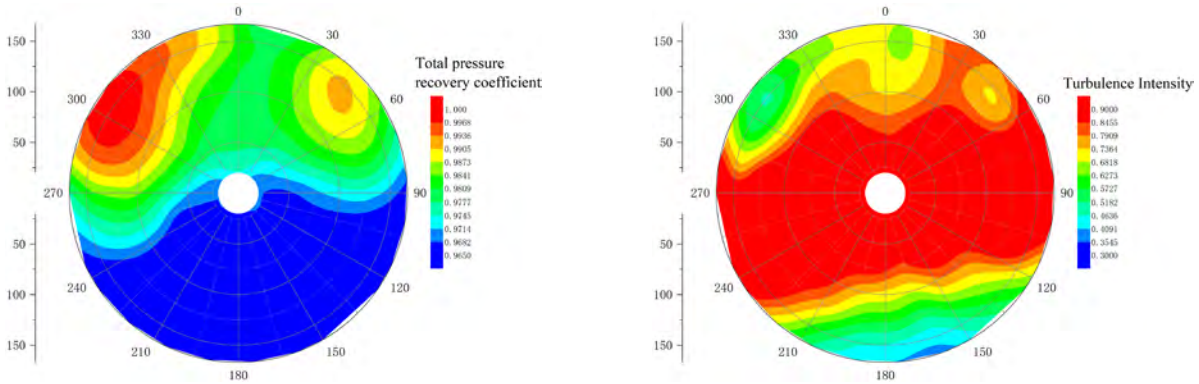

(b) H_{plate}=43mm, θ_{plate}=120°

Figure.8 APBDG's distortion maps for different annular plate heights

Effect of annular plate's circumferential scale on distortion descriptor

Figure.9 illustrates the changes in the steady-state distortion descriptor and turbulence of the APBDG. As shown in the figure, the steady distortion descriptor and turbulence all increase with the annular plate's circumferential angle. The steady-state and dynamic distortion components are corresponding to the circumferential scale. As the circumferential angle increases, the dynamic component of total pressure distortion increases by 60% at most, the corresponding steady-state component increases by 21.6%.

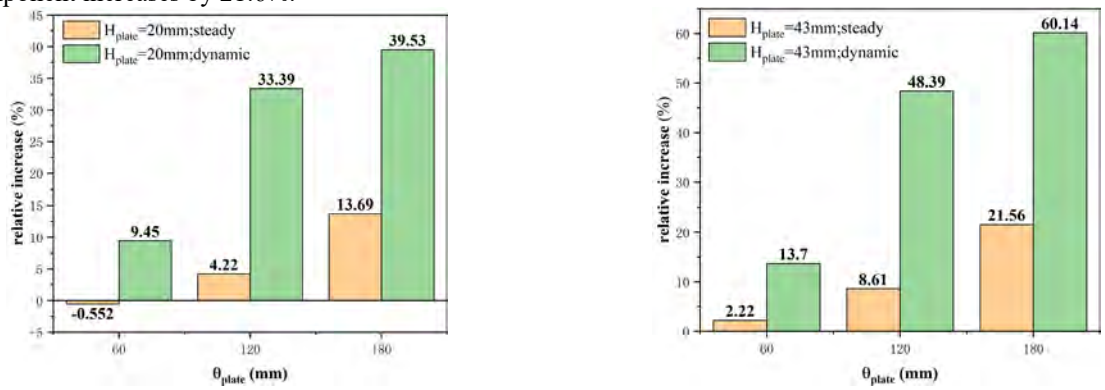

Figure.9 Effect of annular plate circumferential scale on the distortion descriptor's relative increase

Figure.10 demonstrates the relationship between the distortion descriptor and circumferential scale of the annular plate. For the annular plate height of 20mm, the distortion descriptor of the APBDG is insensitive to the circumferential angle. However, at 43mm annular plate height, turbulence increases faster than steady-state distortion for different circumferential angles. The ratio of the steady and dynamic total pressure distortion decreases with the annular plate's circumferential scale.

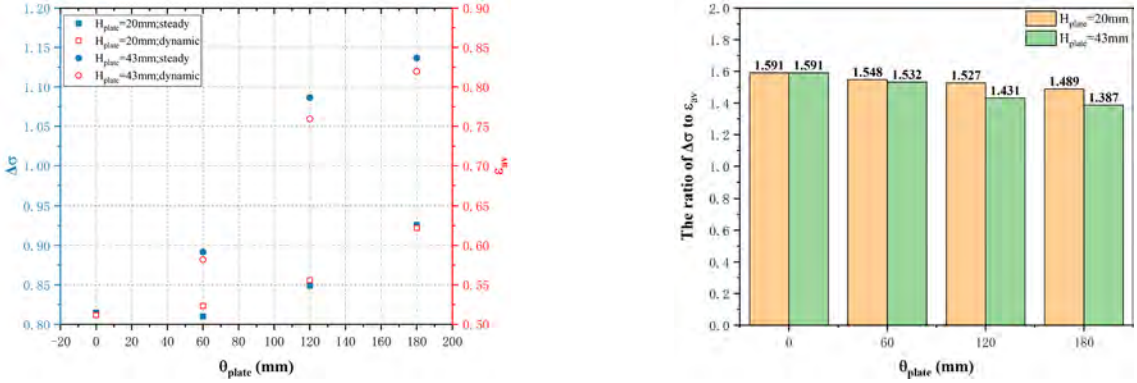

Fig.10 Effect of annular plate circumferential scale on distortion descriptor

Figure.11 displays the distortion patterns of the annular plate at various circumferential angles with a height of 43mm. The total pressure recovery coefficient maps show that the annular plate creates a pressure gradient formation within the center of the high-pressure zone, resulting in a new transition zone, significantly improving the turbulence therein. As the annular plate's circumferential scale increases, the new transition zone's pressure gradient intensifies, and the turbulence intensity further improves. The range of the previous transition region also widens with the circumference scale increasing. While the range of the low-pressure region remains unchanged even the circumferential scale increases. The variation of

the transient region and the low-pressure region indicates that the dynamic component will grow faster than the steady-state component with the circumferential scale increasing.

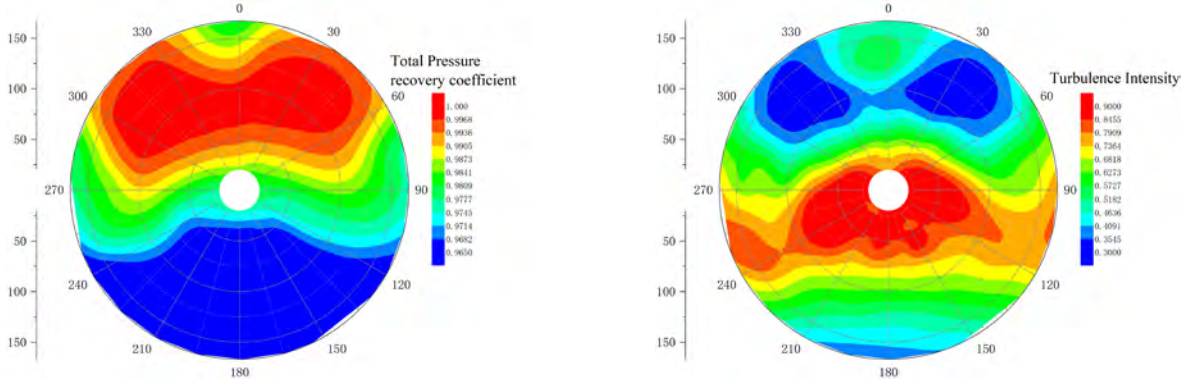

(a) Distortion flowfield generated by the APBDG (θ_{plate}=60° , H_{plate}=43mm)

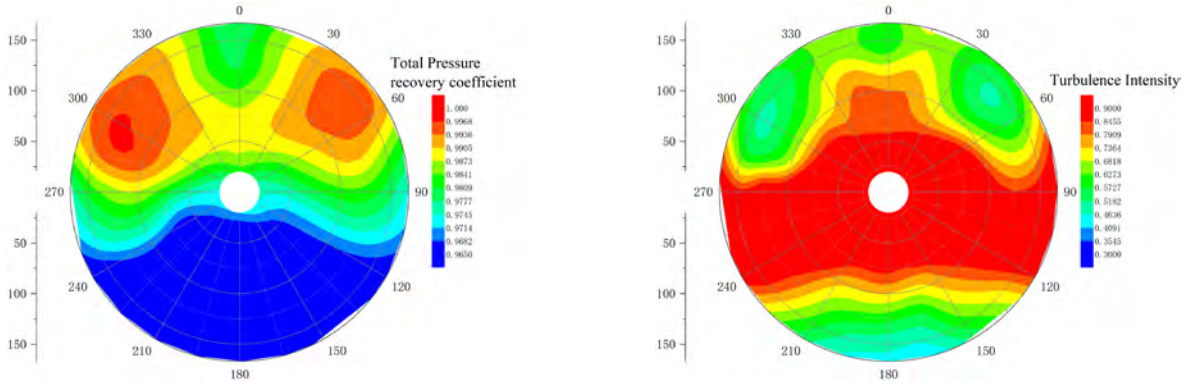

(b) Distortion flowfield generated by the APBDG (θ_{plate}=120° , H_{plate}=43mm)

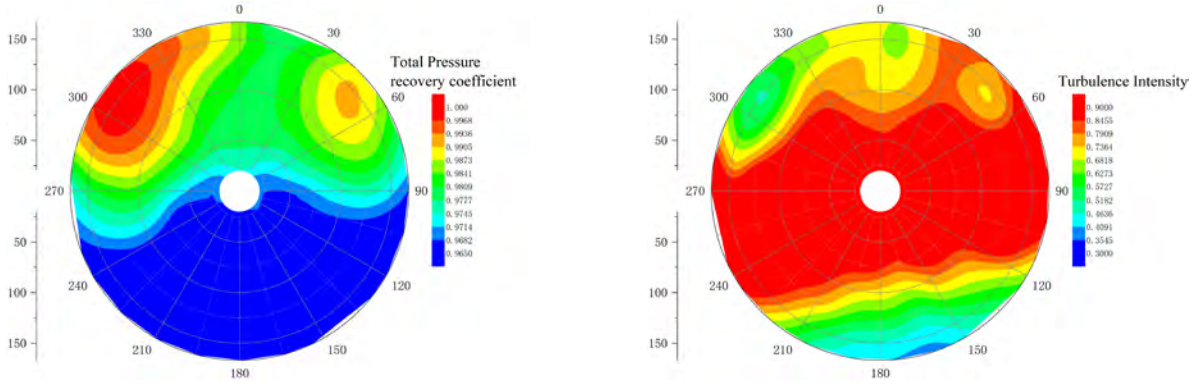

(c) Distortion flowfield generated by the APBDG (θ_{plate}=180° , H_{plate}=43mm)

Figure.11 APBDG's distortion maps for different annular plate circumferential angles

EFFECT OF CYLINDRICAL ROD ON DISTORTION DESCRIPTOR

Effect of cylindrical rod's height on distortion descriptor

Figure.12 depicts the influence of the cylindrical rod's height on the distortion descriptor. The results indicate that an increase in the height of cylindrical rods can lead to the ratio of the steady and dynamic total pressure distortion components decreasing. The steady-state components of total pressure distortion decrease faster than the dynamic components with the rod's height increasing. The results show that the ratio of steady and dynamic distortion reduces by 6.7% mostly, which means that 100mm cylindrical rod has a better ability to adjust the distortion flow field.

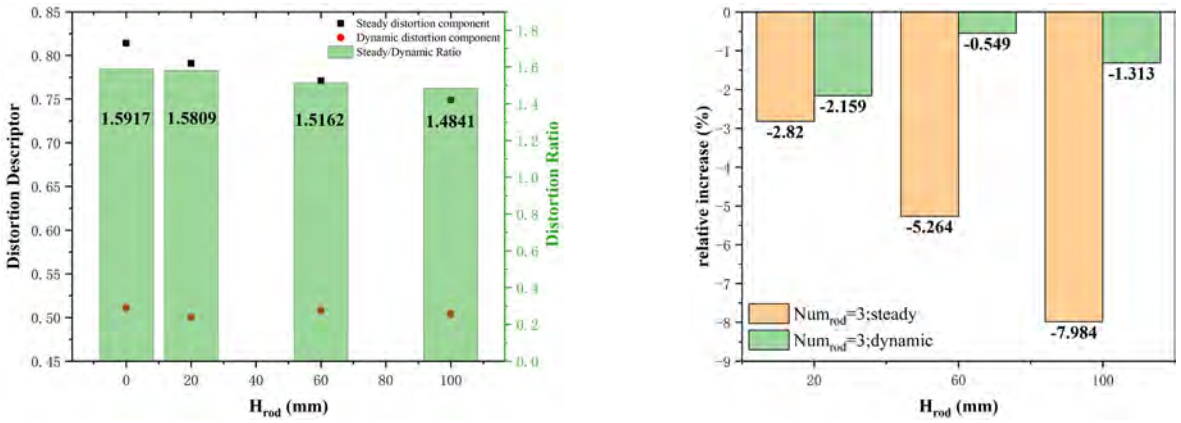

Figure.12 Effect of cylindrical rod's height on distortion descriptor

Fig.13 indicates the influence of the cylindrical rod's height on the distortion flow field. The flow field becomes more uniform when adding the cylindrical rod's height. As the blockage caused by the baffle induces severe speed loss, the cylindrical rod has no ability to generate more strong and powerful turbulence to increase the dynamic components of the total pressure distortion. That is why the patterns seem no significant change.

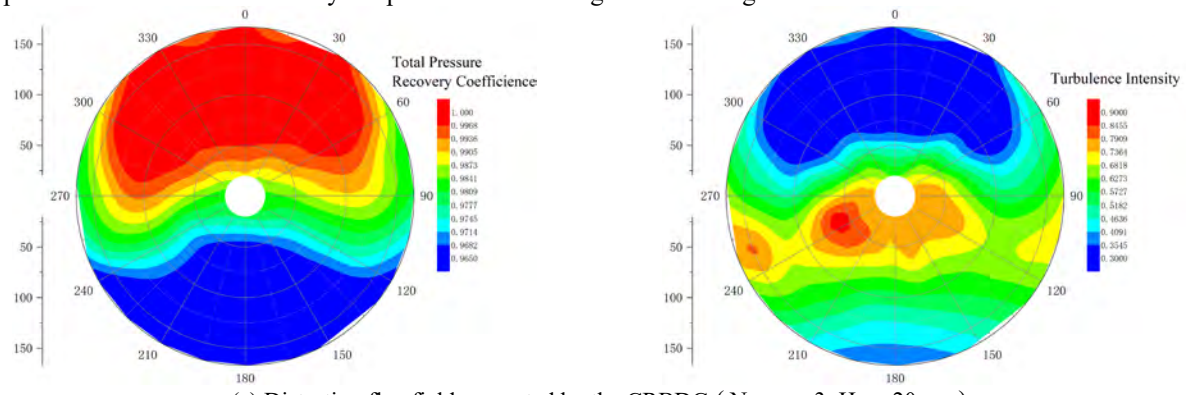

(a) Distortion flowfield generated by the CRBDG (Num_{rod}=3; H_{rod}=20mm)

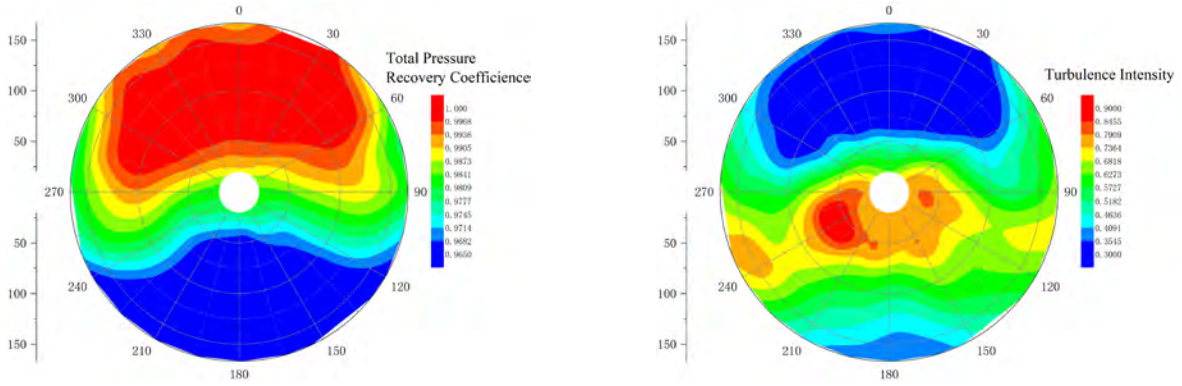

(b) Distortion flowfield generated by the CRBDG (Num_{rod}=3; H_{rod}=60mm)

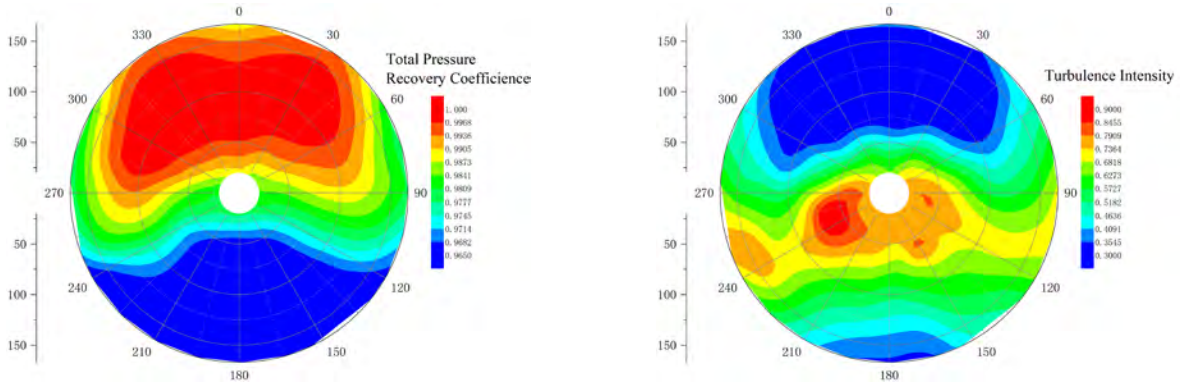

(c) Distortion flowfield generated by the CRBDG (Num_{rod}=3; H_{rod}=100mm)

Figure.13 Distortion patterns of CRBDG for different rod's height

Effect of cylindrical rod's number on distortion descriptor

The cylindrical rod's number is also a key factor influencing the ratio of steady and dynamic components of total pressure distortion. As shown in Figure.14, the steady-state distortion components decrease and the dynamic distortion components increase slightly after adding cylindrical rods. The steady-state distortion descriptor can reduce by 8.18% at most, and the dynamic distortion descriptor can increase by 1.47% at most. The ratio of steady and dynamic components reduces by 9.5% maximally when the rod's number is seven. However, as the blockage induced by the baffle, the dimension of the cylindrical rod is too small to generate stronger turbulence, and the effect of increasing rod's number is not obvious.

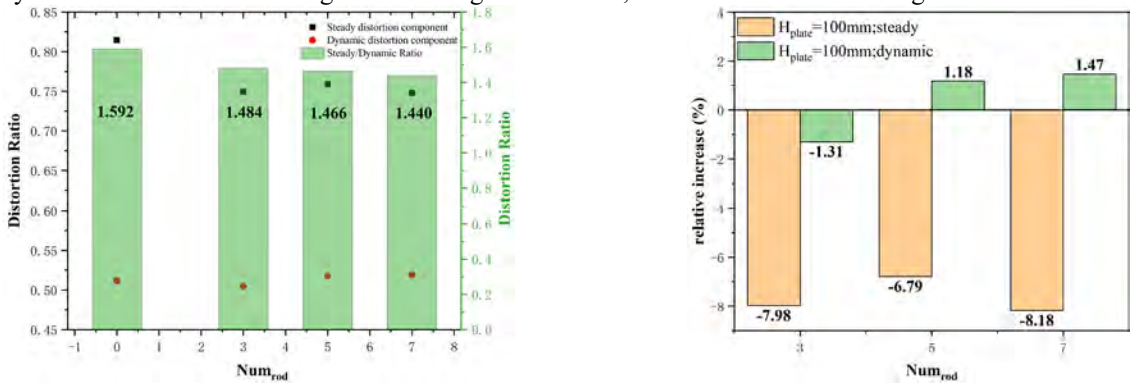

Figure.14 Effect of cylindrical rod's number on distortion descriptor

CONCLUSION

Through a series of indraft wind tunnel tests conducted on the APBDG and CRBDG, this study explores the effects of geometrical parameters of annular plates and cylindrical rods on the flow field characteristics of distortion. It verifies the viability of using combination generators to regulate the steady/dynamic distortion ratio. Based on the experimental results, the conclusions are as follows:

1.The flow field distorted by the baffle exhibits three distinct regions, including the low-pressure region resulting from the blockage of the baffle, the high-pressure region above the baffle devoid of any disturbance, and the transition region formed from the edge of the baffle. Notably, the turbulence intensity within the transition region is the most pronounced, followed by the low-pressure region, with the high-pressure zone displaying the weakest turbulence.

2.The annular plates can engender novel perturbations in flow field, consequently amplifying the intensity of turbulence in the high-pressure zone. The combination of annular plates and the baffle produces a constriction in the flow channel, giving rise to a "throat" effect, which in turn accelerates the fluid in the primary flow zone, augmenting the turbulence intensity in the transitional zone. An increase in the height or circumferential scale of the annular plate will induce an upsurge in the pulsating pressure of the flow field. Upon the selection of the appropriate height and circumferential angle of the annular plate, the minimal ratio of the steady and dynamic components of total pressure distortion is 1.38, which reduces by 12.9% maximally.

3.Cylindrical rods also can adjust the distortion descriptor, but the adjusting ability is limited. The rod's dimension is too small to generate stronger turbulence to improve the dynamic component of total pressure distortion. The steady-state component of total pressure distortion decreases with the rod's height increasing. Adding cylindrical rods can reduce steady-state distortion descriptor, but adding rod's number has little influence on the distortion descriptor, as the speed loss induced by the baffle and the rod's small dimension.

NOMENCLATURE

H	=	baffle/cylindrical rod/annular plate height
L	=	the distance between the rod/plate and baffle
Num	=	cylindrical rod's number
θ	=	circumferential angle
σ	=	total pressure recovery coefficient
$\Delta\sigma$	=	steady circumferential total pressure distortion descriptor
ε	=	turbulence intensity
P	=	pressure
ρ	=	air density
V	=	axial velocity
N	=	number of dynamic total pressure measurement points
t	=	time
T_u	=	sampling time
i	=	ith dynamic total pressure measurement point

Subscript/supscript

rod	=	cylindrical rod
plate	=	annular plate
av	=	averaged
0	=	low-pressure region
1	=	inlet
2	=	outlet
RMS	=	root mean square
*	=	stagnation quantities

SDR = steady/dynamic ratio
APBDG = annular plate baffle distortion generator
CRBDG = cylindrical rod baffle distortion generator

References

Anderson, B, H. and Gibb, J. (1998). Vortex-Generator Installation Studies on Steady-State and Dynamic Distortion, *Journal of Aircraft,* 35(4), pp. 513-520.

Anderson, R. (1983). Aircraft Engine Inlet Pressure Distortion Testing in a Ground Test Facility. 19th Joint Propulsion Conference.

Bowditch, D. and Coltrin, R. (1983). A Survey of Inlet/Engine Distortion Compatibility. 19th Joint Propulsion Conference.

Brimelow, B., Collins, T. and Pfefferkorn, G. (1974). Engine Testing in a Dynamic Environment. 10th Propulsion Conference.

Cramer, K. B. (2002). *Design of a Total Pressure Distortion Generator for Aircraft Engine Testing.* MS. Virginia Polytechnic Institute and State University.

Dipietro,T. (1996). Fundamental Wind Tunnel Experiments for Total Pressure Distortion Generator Concept Selection. Year End Report for Sverdrup Technology.

Eddy, G. L. (2001). *Study of Steady-State Wake Characteristics of Variable Angle Wedges.* MS. Virginia Polytechnic Institute and State University.

Gil-Prieto, D., Macmanus, D. G., Zachos, P. K. and Bautista, A. (2018). Assessment Methods for Unsteady Flow Distortion in Aero-Engine Intakes. *Aerospace Science and Technology,* 72, pp. 292-304.

Gil-Prieto, D., Zachos, P. K., Macmanus, D. G. and Mclelland, G. (2019). Unsteady Characteristics of S-Duct Intake Flow Distortion. *Aerospace Science and Technology,* 84, pp. 938-952.

Hubble, J. and Smith, R. (1979). Evaluation of an Airjet Distortion Generator used to Produce Steady-State, Total-Pressure Distortion at the Inlet of a General Electric F101-GE-100 Turbofan Engine. ARO INC ARNOLD AFS TN.

Kimzey, W. (1965). An Investigation and Calibration of a Device for the Generation of Turbulent Flow at the Inlet of a Turbojet Engine. ARNOLD ENGINEERING DEVELOPMENT CENTER ARNOLD AFB TN.

Kutschenreuter JR, P., Collins, T. and Vier III, W. (1974). P 3G-A New Dynamic Distortion Generator. *Journal of Aircraft,* 11(6)**,** pp. 344-348.

Lazalier, G. and Tate, J. (1970). Development of a Prototype Discrete Frequency, Total-Pressure Fluctuation Generator for Jet Engine/Inlet Compatibility Investigation. Proc. Air Force Airframe Propulsion Compatibility Symposium, AFAPL-TR AFAPL-TR: Air Force Aero Propulsion Lab Technical Report.

Longley, J. and Greitzer, E. (1992). Inlet Distortion Effects in Aircraft Propulsion System Integration. Steady and Transient Performance Prediction of Gas Turbine Engines. Advisory Group for Aerospace Research and Development(AGARD).

Mistry, C. S. and Pradeep, A. (2013). Investigations on the Effect of Inflow Distortion on the Performance of a High Aspect Ratio, Low Speed Contra Rotating Fan Stage. Turbo Expo: Power for Land, Sea, and Air.

Oates, G. C., Sherman, D. A. and Motycka, D. L. (1969). Experimental Study of Inlet-Generated Pressure Fluctuations. Airframe/Propulsion Compatibility Symposium.

Overall, B. (1976). Evaluation of an Airjet Distortion Generator Used to Produce Steady-State, Total-Pressure Distortion at the Inlet of Turbine Engines. Arnold Engineering Development Center Arnold AFB TN.

Overall, B. and Harper, R. (1977). The Airjet Distortion Generator System-A New Tool for Aircraft Turbine Engine Testing. 13th Propulsion Conference.

Plourde, G. and Brimelow, B. (1969). Pressure Fluctuations Cause Compressor Instability. Proceedings of the Air Force Airframe-Propulsion Compatibility Symposium.

SAE. (2017). *Inlet Total-Pressure-Distortion Considerations for Gas-Turbine Engines*. Socity of Automotive Engineers, S-16 Turbine Engine Inlet Flow Distortion Committee.

Smith JR, R. E. (1996). Marrying Airframes and Engines in Ground Test Facilities-An Evolutionary Revolution. *Journal of Aircraft*, 33(4), pp. 649-679.

Tanguy, G., Macmanus, D. G., Garnier, E. and Martin, P. G. (2018). Characteristics of Unsteady Total Pressure Distortion for a Complex Aero-Engine Intake Duct. *Aerospace Science and Technology*, 78, pp. 297-311.

Van Deusen, E. and Mardoc, V. (1972). Distortion and Turbulence Interaction-A Method for Evaluating Engine Inlet Compatibility. *Journal of Aircraft*, 9 (1), pp. 16-22.

Xu, D., He, C., Sun, D. & Sun, X. (2021). Stall Inception Prediction of Axial Compressors with Radial Inlet Distortions. *Aerospace Science and Technology,* 109**,** pp. 106433.